COURSE 3

RECENT EXPERIMENTS ON MULTIPLE SCATTERING AND LOCALIZATION OF LIGHT

Georg Maret

Institut Charles Sadron, CNRS
6, rue Boussingault
F-67083 Strasbourg - Cedex France

E. Akkermans, G. Montambaux, J.-L. Pichard and J. Zinn-Justin, eds.
Les Houches, Session LXI, 1994
Physique Quantique Mésoscopique
Mesoscopic Quantum Physics

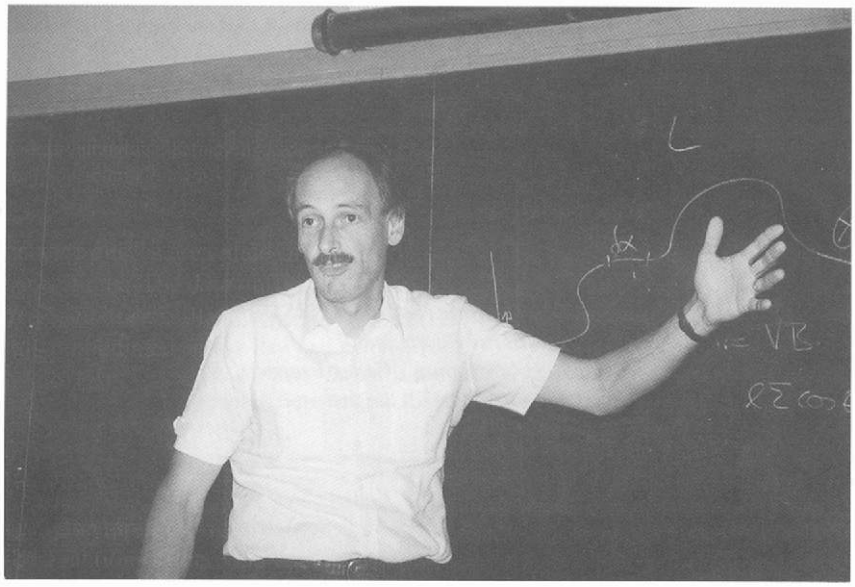

Contents

1. Introduction

In this lecture, an attempt is made to review parts of the development of optical multiple scattering during the past decade [1–5]. Emphasis will be on experimental observations and on a discussion of the underlying physics in simple terms. Multiple light scattering is not only of interest because of fundamental issues such as localization of classical waves, but also since many direct applications of the discussed principles emerge. In fact, almost all visible objects in nature *multiply* scatter light: white paints, milk, snow or clouds are examples with negligible absorption, whereas colored objects like leaves, wood or stones have rather strong absorption bands somewhere in the visible. Many features of multiple light scattering can be transposed to other classical waves such as (ultra)sound, heat or microwaves diffusing through random media. This has various practical implications, for example in material testing and remote sensing. Analogies and differences of light and *electron* transport are briefly summarized in section 4. One of the beauties of the optical case is that many things – like all features of single scattering or the transport mean free path of light – can be calculated in general.

1.1. Single scattering

The following introduction to single light scattering for dielectric particles with radius R smaller (Rayleigh scatterers) and larger (Mie scatterers) than the optical wavelength λ originates from two classical books [6,7].

1.1.1. Rayleigh scattering, ($R \ll \lambda$):

Light with electric field amplitude $\boldsymbol{E}_o$ linearly polarized along $\boldsymbol{x}$ incident along $\boldsymbol{z}$ generates an induced dipole moment inside the particle, which in turn radiates off an electromagnetic dipole field. With ψ being the angle between the scattering direction $\boldsymbol{r}$ and $\boldsymbol{x}$, the scattered intensity is

$$I_s = 16\pi^4 \frac{R^6}{r^2\lambda^4}\left(\frac{m^2-1}{m^2+2}\right)^2 E_o^2 \sin^2\psi.$$

r is the distance from the scatterer and $m = n_1/n_2$ the ratio of the refractive index of the particle (index 1) and the surrounding medium (index 2). For spheres, m relates to the polarizability α by $\alpha = (m^2-1)/(m^2+2)R^3$. Because $I_s \propto \lambda^{-4}$, clear sky appears blue. Note that the scattered intensity increases with the square

of the volume V of the particles. Defining the scattering angle θ_s between $\boldsymbol{z}$ and $\boldsymbol{r}$ one immediately finds the donut shaped angular intensity distribution of I_s for unpolarized incident light $I_s \propto (1 + \cos^2\theta_s)/2$ and a degree of polarization $P = (1 - \cos^2\theta_s)/(1 + \cos^2\theta_s)$. The scattering matrix $\mathbf{S}$, connecting the horizontally and vertically polarized scattered fields with the horizontally and vertically polarized incident fields has the diagonal form

$$\begin{pmatrix} S_2(\theta_s) & S_3 \\ S_4 & S_1 \end{pmatrix} = ik^3\alpha \begin{pmatrix} \cos\theta_s & 0 \\ 0 & 1 \end{pmatrix}$$

Angular integration of I_s gives the total scattering cross section

$$C_s = \frac{24\pi^3 V^2}{\lambda^4}\left(\frac{m^2-1}{m^2+2}\right)^2$$

and division by the geometric cross section πR^2 the "efficiency factor" Q_s as a function of the size parameter $x = kR$.

$$Q_s(x) = \frac{8}{3}x^4\left(\frac{m^2-1}{m^2+2}\right)^2 \tag{1.1}$$

1.1.2. Rayleigh–Debye–Gans scattering ($kR|m-1| \ll 1$):
This simple scheme can be generalized to larger particles, which are considered as an ensemble of small volume elements acting like Rayleigh scatterers. The total scattered field is expressed as the coherent sum of the fields from the volume elements located at $\boldsymbol{r}_i$. As long as the incident plane wave front is not distorted by the presence of the other volume elements ($x|m-1| \ll 1$) the phase factors between two volume elements are simply $e^{-i\boldsymbol{q}_s(\boldsymbol{r}_i-\boldsymbol{r}_j)}$ with the scattering vector $\boldsymbol{q}_s = 2\boldsymbol{k}\sin(\theta_s/2)$. The scattered intensity therefore becomes $I_s = k^4V^2/(4\pi^2r^2)|m-1|F(\theta_s)$ which is angular dependent because of the angular dependence of the form factor $F(\theta_s) = V^{-2}|\int e^{-i\boldsymbol{q}_s(\boldsymbol{r}_i-\boldsymbol{r}_j)}\,dV|^2$. For a homogeneous sphere, for example, one obtains

$$F(\theta_s) = \left[\frac{3(\sin q_sR - q_sR\cos q_sR)}{(q_sR)^3}\right]^2$$

and

$$Q_s = (m-1)^2\left[\begin{array}{c}\frac{5}{2} + 2x^2 - \frac{\sin 4x}{4x} - \frac{7}{16x^2}(1-\cos 4x) + \\ +(\frac{1}{2x^2} - 2)(\gamma + \log 4x - Ci(4x))\end{array}\right], \tag{1.2}$$

γ being Euler's constant and Ci the cosine integral. For increasing x Q_s deviates from the one for Rayleigh scattering and becomes, for $x \gg 1$, $Q_s = 2(m-1)^2x^2$. Evidently, in the Rayleigh Gans regime, scattering is always weak ($Q_s \ll 1$), whatever the particle size. Strongly light scattering samples of reasonable size

can therefore only be achieved by using particles with refractive index mismatch $m \geq 1.5$.

1.1.3. Mie scattering (any kR, any m):
The general theory of scattering of light from homogeneous dielectric spheres is due to Mie and Debye. Based on this work, a vast literature has developed treating particles of various shapes, inhomogeneous particles and absorption. Fully analytical solutions exist only for certain limiting cases, and the derivation of Q_s is sketched here only for the simplest case of a homogeneous sphere without absorption.

The general problem is to solve the electromagnetic wave equations for the incident wave, the wave inside the particle and the scattered wave, the different components of the electric and magnetic fields of the light being connected through the boundary conditions at the surface of the sphere. By introducing the electric and magnetic Hertz potentials Π_1, Π_2 in the usual way, the problem reduces to solving the *scalar* wave equations $\nabla^2\Pi + k^2\Pi = 0$ for Π_1 and Π_2. The $\Pi's$ can be expressed as $\Pi = R(\theta_s)P_n^{(m)}(\cos\theta_s)\Phi(\phi)$, where $R(\theta_s)$, $P_n^{(m)}(\cos\theta_s)$ and $\Phi(\phi)$ are Ricatti–Bessel, associated Legendre and $\sin, \cos$ functions, respectively. Writing the general solutions for the incident, internal and scattered wave as series expansions $\Pi = \sum_{n=0}^{\infty}\sum_{m'=-n}^{n}(c_n\psi_n + d_n\chi_n)P_n^{(m')}(a_{m'}\cos\phi_{m'} + b_{m'}\sin\phi_{m'})$ and using the boundary conditions at the surface of the sphere, one obtains expressions for the Mie coefficients a_n, b_n, c_n and d_n, which only depend on the Ricatti–Bessel functions $\psi_n, \psi_n', \chi_n, \chi_n'$ of order n. This gives the far field scattered amplitudes S_1 and S_2 and the corresponding intensities as a series in n. Like in Rayleigh–Gans scattering, the scattered intensity decreases with increasing scattering angle θ_s and becomes very small for $x > 1$. Particles larger than a wavelength scatter mostly forward. With increasing refractive index mismatch between sphere and outer medium, the zeros of the Rayleigh–Gans form factor $F(\theta_s)$ become more and more filled up with scattered intensity, since the wave fronts inside the sphere are more and more distorted as compared to free space, which prevents the destructive interference of *all* scattered waves at particular angles. Finally, the efficiency factor is

$$Q_s = C_s/\pi R^2 = \frac{2\pi}{x}\sum_{n=1}^{\infty}(2n+1)\left[a_n^2 + b_n^2\right] \tag{1.3}$$

For anisotropic scatterers, it will be useful to introduce the transport cross section C_t (or radiation pressure cross section), which differs from the scattering cross section C_s by the amount of scattered intensity which does not change direction on scattering. $C_t = C_s(1 - \langle\cos\theta_s\rangle_{\theta_s})$. Here $\langle\cdots\rangle_{\theta_s}$ denotes angular integration over the form factor $F(\theta_s)$.

1.2. Random walks and classical diffusion

Let us now consider scattering from more than one particle. We first discuss an ideal gas of non-interacting scatterers at a small particle density ρ such that the average inter-particle distances are much larger than λ. For the moment we do not worry about interference effects *between* scatterers, although they are very important. Due to the presence of many scatterers, more and more of the incident light beam is scattered as it proceeds through the cloud of particles, the incident intensity decays exponentially on the length scale $l_s = 1/C_s\rho$. If the medium has a size $L \gg l_s$ there is essentially no directly transmitted beam, virtually all transmitted light is multiply scattered: one can not see an object hidden behind the medium, since the directly transmitted beam is too weak compared to the scattered light. Using C_t one can define another length scale, the transport mean free path $l_t = 1/C_t\rho$ which is the length over which the incident intensity spreads into all directions (loss of memory of the direction of $\boldsymbol{k}$). l_s and l_t are identical for completely isotropic scattering, but may differ by more than an order of magnitude for Mie scatterers. For $L \gg l_t$ light propagates diffusively on scales $> l_t$ and except for a surface layer of thickness of order l_t the flux of light intensity is essentially isotropic: Deep inside a thick cloud, it is impossible to figure out the direction of the sun. There are various ways to describe this type of light transport, but as most of them are analogous to those of electron transport widely discussed in this school, I adopt the simple and very physical point of view of random walk of photons or diffusion of light intensities. This does not include polarization effects, but provides a good semi-quantitative account for many experiments. A general overview on light transport and radiative transfer is given in [8] and [9]. Let $P(\boldsymbol{r}, \boldsymbol{r}', t)$ be the probability that a photon is scattered from $\boldsymbol{r}$ to $\boldsymbol{r}'$ within a time t. $P(\boldsymbol{r}, \boldsymbol{r}', t)$ can also be considered as the diffusing light intensity and obeys the diffusion equation

$$(D\nabla^2 + \frac{\partial}{\partial t})P(\boldsymbol{r}, \boldsymbol{r}', t) = \delta(\boldsymbol{r} - \boldsymbol{r}')\delta(t). \tag{1.4}$$

$D = cl_t/3$ is the diffusion constant and c the speed of light. The solution for an infinite medium (with $P = 0$ at $\rho' = |\boldsymbol{r} - \boldsymbol{r}'| = \infty$) is

$$P(\boldsymbol{r}, \boldsymbol{r}', t) = \frac{1}{(4\pi Dt)^{3/2}} e^{-\frac{\rho'^2}{4Dt}} \tag{1.5}$$

Converting from time to space by $Dt = l_t s/3$, $s = ct$ being the contour length of the diffusion path, $P(\rho', s)$ is the probability of a random walker to be at a linear distance ρ' after a walk of length s. $P(\rho', s)$ is easily calculated for different bounded scattering media using the method of images. The key of this is that paths which cross the interface once between inside and outside the medium never

return, since the corresponding walker escapes. This mimics an absorbing wall at the interface. All paths from a starting point $\boldsymbol{r}$ (inside) to the mirror image $\boldsymbol{r}''$ (outside) of the ending point $\boldsymbol{r}'$ (inside) cross the interface once. Thus for a semi-infinite half-space $P = P(\rho', s) - P(\rho'', s)$. As an example, locating $\boldsymbol{r}$ and $\boldsymbol{r}''$ at a distance l_t from the interface, one obtains P using eq. (1.5) and by integration over ρ' the total path length distribution for reflection from a semi-infinite medium

$$P(s) = \frac{4\pi l_t^2}{(\frac{4\pi}{3} s l_t)^{3/2}} \tag{1.6}$$

In the case of transmission through an infinite multiple scattering slab of thickness $L \gg l_t$, an infinite series of multiple images has to be considered due to the presence of the two parallel mirror planes. One obtains

$$P(s) = \frac{2}{L} \sum_{n=1}^{\infty} \exp(-\frac{n^2\pi^2 s l_t}{3L^2}) \sin\frac{n\pi l_t}{L} \sin\frac{n\pi(L-l_t)}{L}. \tag{1.7}$$

$P(s)$ is the central function required for the calculation of various experimentally accessible quantities discussed below. It reflects the geometry of the scattering medium: In reflection, short paths of a few l_t are more probable than long paths, but the decay ($s^{-3/2}$) is slow, whereas in transmission both very short and very long paths have exponentially small probability and the most probable path length is of order L^2/l_t. $P(s)$ can be directly determined from the temporal broadening of a short (psec) incident laser light pulse.

The above discussion makes clear why the intensity scattered from a white object is essentially independent of the angle of observation both in reflection and transmission: Memory of direction is lost on the random walk step length l_t and basically all paths start and end within l_t from the interface. Integration of eq. 1.6 and eq. 1.7 over s gives the total reflectivity $R \to 1$ and the total transmission $T \to l_t/L$ for $L/l_t \to \infty$. Absorption is easily incorporated as an exponential attenuation e^{-s/l_a} along the contour s, l_a being the absorption length.

1.3. Classical wave interferences, speckles

In fact, when *laser* light is scattered from a white wall or a sheet of paper the scattered intensity is not at all independent of the angle of observation but strongly fluctuates on a angular scale of typically 10^{-3} to $10^{-6} rad$. This granular scattering pattern, in optics known as *speckle*, is characterized by a high degree of randomness: Angular correlations only extend over the size of individual spots and the intensity varies widely from spot to spot. Closer analysis reveals that the intensity distribution function is an exponential $p(I) = e^{-I/\langle I\rangle}$ and the angular correlation function decays with a Gaussian of width λ/W, where W is the beam waist [10].

Both of these features are characteristic for an interference pattern of a large number of scattered fields with random phases (Gaussian distribution of fields) [10]. In multiple light scattering, the mutual phase shifts between fields scattered along different paths are generally much larger than λ because of the broad distribution $P(s)$ of path lengths s. As the coherence length of laser light (typically 0.01 to $100m$) is much longer than most path length differences, the fields add *coherently* at the detector. The radiating surface zone of the sample can be considered as a planar source of linear dimension W of many random fields and the scattered far field pattern is just the 2D Fourier transform of this zone. From this point of view, the speckle pattern does not tell us much about the sample except that the latter generates random fields, but it really is a complicated interferometric fingerprint of the positions of the scatterers. So, interferences *are* important in multiple scattering of laser light, and the reason why the description of section 1.2 was nevertheless successful for about a century [11] is that coherence lengths of natural and artificial light other than laser light are much shorter than typical diffusion paths. The above picture obviously also holds for laser light when speckle patterns are averaged, for instance by motion of the scatterers or changes of λ. In other words, interferences between fields scattered along different paths do not contribute to the scattered intensity when proper ensemble averaging is made. The latter condition requires no correlations of the fields scattered along the different paths, an assumption usually very well satisfied, but which is in fact not completely correct (see section 2.5).

We have seen in section 1.1, that a single light scattering event modifies the polarization state. Therefore, the polarization state of the incident light changes in the process of multiple scattering in a complicated way determined by the geometry of the paths. Hence, for a thick sample ($l_t \ll L$), the transmitted light is completely depolarized. More precisely, in the case of uncorrelated paths, the individual speckle spots have well defined but mutually uncorrelated polarization states [12]. Multiple scattering speckle patterns consist of two orthogonally polarized uncorrelated gaussian speckle patterns.

2. Coherent backscattering and localization

2.1. Weak localization and enhanced backscattering

This section discusses the fact (first realized in solid state physics more than 30 years ago) that one constructive interference survives the above ensemble averaging over different representations of disorder. Let us consider first purely elastic scattering, i.e. no motion of scatterers. In this case, as evident from fig. 1a, all phase shifts the light wave accumulates along a given scattering path (between

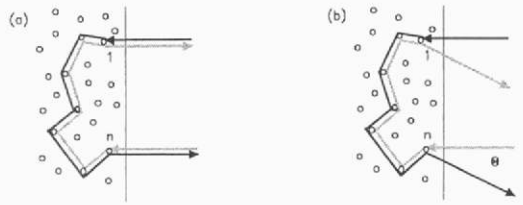

Fig. 1. The origin of coherent backscattering is constructive interference between reversed multiple scattering paths

first and n^{th} scattering event) exactly equal the phase shifts along the *same* path passed in the opposite direction (n to 1). Therefore, for a plane wave such as an expanded laser beam incident on a thick multiple scattering slab, these two waves constructively interfere in the backscattering direction. It is important to realize that this constructive interference occurs for all pairs of "reversed" paths whatever their conformation and whatever the distance between first and last scatterer. Therefore, in contrast to the speckle interferences, it survives averaging over different sets of positions of the scatterers. The minimum number of scattering events in a path required for this effect to occur is $n = 2$. If single backscattering has negligible contribution to the total intensity reflected from the sample, *all* reflected light contributes to this interference. As two waves interfere constructively, the intensity is enhanced by a factor 2 right in backscattering. Because of the total coherence between the "reversed" paths, this effect is usually called "coherent" backscattering, despite of the fact that light from different paths is completely incoherent. Obviously, for a given position of first and last scatterer of a path, higher order constructive and destructive interferences occur at angles off backscattering (fig. 1b). However, these angles depend on the distance between first and last scatterer and because of the broad distribution of distances all higher order interference effects average out. Constructive interference therefore only exists in a narrow range of angles around backscattering, in fact for angles smaller than the angle corresponding to the shortest typical distance between path ends. The shortest paths (on average) correspond to double scattering and, consequently, the shortest typical distance is of order l_t. It follows that the typical width of the cone is of order λ/l_t [13].

Although the fundamental mechanism of coherent backscattering of electromagnetic waves was discussed already in 1969 [14,15], its clear experimental observation was only made in 1984–85 [16–18]. These first experiments were performed by illuminating concentrated aqueous suspensions of sub-micron size colloidal latex particles at about 10% volume fraction with visible laser light and monitoring the backscattered intensity through a semi-transparent beam splitter. The angular width of the cone was about 0.1^o in those samples and varied linearly

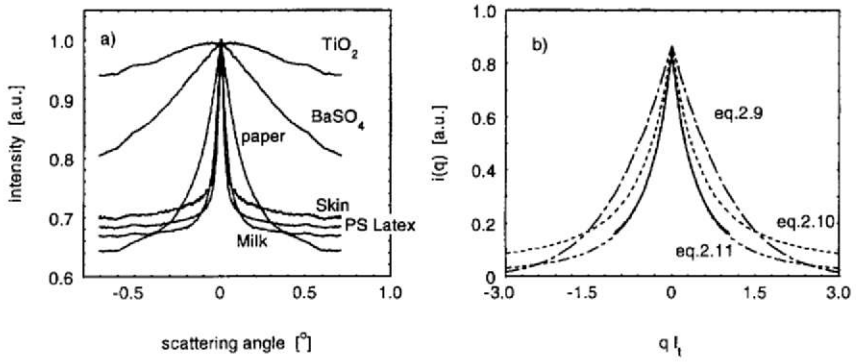

Fig. 2. (a) Coherent backscattering cones of various samples. (b) Comparison of theories of the angular shape of the cone with data (continuous line) on pressed powder of $BaSO_4$ μ-crystals.

with the concentration of scatterers ($l_t \propto \rho^{-1}$), whereas its height was constant, as expected*. Because of instrumental improvements (e.g. linear and 2D detector arrays) it rapidly became clear, that cones can be seen from most turbid media even in cases of strong absorption. A few examples are shown in fig. 2a.

In these samples the excess intensity scattered into the cone is small (of order $(\lambda/l_t)^2/2\pi$) compared to the diffusely reflected "incoherent" light. As a consequence, the total transmission through a finite thickness sample is slightly decreased, by $1-(\lambda/l_t)^2$, below the classical transmission l_t/L in the absence of coherent backscattering, since the sum of reflected and transmitted photon flux must be conserved*. This is very analogous to weak Anderson localization of *electrons* and, therefore, the coherent backscattering effect of light is sometimes called "weak localization" of light.

2.1.1. Angular dependence

Fig. 2a clearly reveals the peculiar shape of the backscattering cone which has a triangular tip and a slow angular decay at the wings. There are various ways to account theoretically for this shape (see e.g. [19–22], but all approaches discussed so far are approximate for typical samples studied: The high volume fractions of scatterers imply significant positional correlations, their large size requires Mie-scattering, which does not properly account for the sometimes irregular shape, and the fact that large parts of the backscattered light has only experienced a few scattering events implies failure of the diffusion approximation. Nevertheless, the cross features of the cone, i.e. width and shape, agree surprisingly well with a simple semi-empirical theory [19], which has, in addition, the benefit of

* But smaller than two for various instrumental reasons as discussed below.
* In non-absorbing media.

being particularly transparent physically. It assumes scalar waves (no polarization), isotropic (Rayleigh) scattering ($l_s = l_t$) and the diffusion approximation to hold even close to the surface of the sample. Because all internal phase shifts along the reversed scattering paths are equal, the contribution of a path starting at $\boldsymbol{r}$ and ending at $\boldsymbol{r}'$ to the coherent intensity is simply given by the phase factor $\cos(\boldsymbol{q}(\boldsymbol{r} - \boldsymbol{r}'))$, $\boldsymbol{q} = \boldsymbol{k_i} + \boldsymbol{k_o}$ being the scattering wave-vector with respect to backscattering. $\boldsymbol{k_i}$ and $\boldsymbol{k_o}$ denote the wave-vector of the incident and out-going detected light, respectively, and near backscattering $|\boldsymbol{q}| = \frac{2\pi}{\lambda}\theta$ with θ being the scattering angle with respect to backscattering. To obtain the total angular dependence of the cone, we have to evaluate the sum over these phase factors, weighted by how much light entering at $\boldsymbol{r}$ leaves at $\boldsymbol{r}'$. This weight is given by $P = P(\rho', s) - P(\rho'', s)$ above (see also [23]). In other words, the angular dependence $i(q)$ of the cone is just the Fourier transform of P. Let us further simplify the problem and assume that all scattering paths start and end at a distance l_s from the interface inside the sample. Then, for random paths of length s, $P(\rho', s)$ is a Gaussian of width $\langle\rho^2\rangle = 4l_t s/3$ and, the Fourier transform of this Gaussian being a Gaussian in q, $i(q)$ can be written as a sum over s

$$i(q) = \frac{\int_{l_t}^{\infty} P(s) e^{-q^2 l_t s/3}\, ds}{\int_{l_t}^{\infty} P(s)\, ds}. \tag{2.1}$$

With $P(s)$ for a semi-infinite slab from eq. (1.6) we obtain

$$i(q) = \frac{-3}{2\sqrt{27}} q l_t (2\sqrt{\pi} + \Gamma(-\frac{1}{2}, 0, \frac{q^2 l_t^2}{3})) = 1 - \sqrt{\frac{\pi}{3}} q l_t + \frac{1}{3} q^2 l_t^2 + \cdots \tag{2.2}$$

This simple theory accounts for both the triangular θ-dependence of the cone near backscattering ($ql_t \ll 1$) and the scaling of its width with ql_t since contributions of long scattering paths, well described by the diffusion approximation, dominate the angular dependence at small ql_t. However, with increasing ql_t, eq. (2.2) becomes less reliable because of the increasing contributions of short paths. Their weight is not correctly described by eq. (1.6) which originates (like eq. (2.1) itself) from the diffusion picture. In addition, the diffusion approximation breaks down near the boundary of the slab, or provides an unphysical boundary condition with non-vanishing diffusive photon flux within a layer of about l_t thickness *outside* the sample [8]. Finally, the conversion of the incident propagating light beam into diffusive flux does not simply occur at a single distance l_t inside the sample. Fig. 2b shows – for comparison with eq. 2.2 – two slightly different expressions by Akkermans et al. [19,20] obtained by using the condition of vanishing diffus-

ive flux a distance γl_t outside the sample and $\gamma = 0.7$. They are, respectively, for start and end points of diffusion paths at a fixed distance l_t inside the sample

$$i(q) = \frac{1 - e^{-2(1+\gamma)ql_t}}{2(1+\gamma)ql_t} = 1 - (1+\gamma)ql_t + \cdots \tag{2.3}$$

and for an exponential distribution of the latter

$$i(q) = \frac{1}{2.4(1+ql_t)^2}(1 + \frac{1 - e^{-2\gamma ql_t}}{ql_t}) \tag{2.4}$$

Ozrin [22] has given recently an expression for scalar waves and anisotropic scatterers based on the exact solution of the radiation transfer equation [8,9]. These and other expressions all reproduce the linear θ-dependence at small θ. However, they provide somewhat different initial slopes and substantially differ at large θ because of the different description of the low order multiple scattering. For typical samples such as aqueous suspensions of colloidal particles or the $BaSO_4$ powder of fig. 2, eq. 2.4 [19] agrees surprisingly well with the data up to $ql_t \approx 1$, experimental γ-values being between 0.6 and 0.7 [19,24–28]. The influence of internal reflections on the cone shape is discussed in section 2.1.3.

2.1.2. Absorption and finite sample size

The description of $i(q)$ in terms of contributions of different path lengths allows very easily to include the effects of absorption [24,29] and finite geometry of the sample [29,30]; they only affect the form of $P(s)$ to be used in eq. 2.1. Absorption attenuates the intensity scattered along paths of length s according to e^{-s/l_a}. Both integrands in numerator and denominator of eq. 2.1 are affected by this attenuation factor in the same way and hence the enhancement factor at $q = 0$ remains unchanged ($i(0) = 1$). In other words, the incoherent scattered intensity, i.e. the background seen outside the cone, is lowered by exactly the same amount than the coherent intensity at $q = 0$. The angular shape of $i(q)$, however, becomes absorption dependent, since long paths contributing essentially to small angles are attenuated more than short paths. The numerator of eq. 2.1 retains the same functional form, if $q^2 l_t/3$ is replaced by $(q^2 l_t/3 + 1/l_a)$. For large θ, $i(q)$ is unchanged, but the tip of the cone is rounded off below an absorption dependent cut-off angle given by $q_a = \sqrt{3/l_a l_t}$. We immediately see that the decrease of the incoherent background (denominator in eq. 2.1) decays as a function of q_a in exactly the same way as $i(q)$ as a function of q for no absorption ($q_a = 0$). Both the absorption induced rounding of the tip and the analogy between $i(q, 0)$ and $i(0, q_a)$ have been quantitatively verified [24].

The effects of finite sample size is also described by a modified $P(s)$. For a very extended slab of thickness L, the intensity in paths of length $s \gg L^2/l_t$ becomes exponentially small, since the light scattered along very long paths is

lossed by escape on the transmission side. Inspection of eq. 1.7 shows that $P(s)$ is essentially damped by $\exp[-(\pi^2 l_t/3L^2)s]$ and hence the corresponding reduced cut-off angle of the backscattering cone is $q_L \approx \pi/L$. This has also been verified experimentally [29,30].

2.1.3. Internal reflections

In an experiment, light crosses the interface between the scattering medium and its surroundings (air, container, optical fiber, ...) on the way in and out. Since the scattering medium and its surroundings generally have different average refractive indices a finite fraction of the diffusing light hitting the sample interface from the inside is reflected back into the medium. This effect can be described by a correction of $P(s)$. The diffusing light re-injected into the sample after internal reflection adds path length to all paths. Therefore the cone width is expected to decrease. A first description of internal reflections assuming an angular-independent average reflectivity R was made [31,32] within the frame of the diffusion approximation. Both models predict a substantial narrowing of the cone with increasing R. The work of Zhu et al. [33], which is corroborated by their experiments on speckle correlation functions, suggests that the major effect of internal reflections is a correction of γ by an additive factor $2(1 + R)/3(1 - R)$. In the limit of small and large index mismatch, this result is in good agreement with a recent theory based on radiation transfer [34] for point-like scatterers and scalar waves. The influence of glass windows in front of the multiple scattering sample on the angular shape of cones was studied [35] both experimentally and by numerical simulations. The internal reflection from the glass–air interface which is stronger than the reflection from the sample-glass interface gives rise to a discontinuity of the cone slope at a characteristic scattering angle related to the thickness of the window. This work and simulations [36] reveal that diffusion theories are actually very accurate for sufficiently thick samples.

2.1.4. Enhancement factor

In the early measurements of the coherent backscattering cones on colloidal suspensions [16–18] the observed tip height was between 10% and 60% above the incoherent background intensity rather than the expected 100% corresponding to an enhancement factor of 2. Further experimental work has revealed various reasons for this: light scattered from optical components, single scattering and multiply scattered light from outside the illuminated sample area all increase the incoherent background, but do not contribute to the cone, therefore decreasing the enhancement factor. The latter effect becomes particularly pronounced for wide angle internally reflected light [35]. Limited angular resolution is a problem for narrow cones (typically $< 0.01^o$). Recently, in a very careful experiment, Wiersma et al. [28] have shown an enhancement factor of 2.00 ± 0.01 in samples

with $k_0 l_t \gg 1$ and have argued that recurrent multiple scattering events* which become more probable for $k_0 l_t \to 1$ could be responsible for the observed lowering of the enhancement for small $k_0 l_t$.

2.2. *Weak positional correlations of scatterers*

Our description of multiple light scattering was restricted so far to low volume fractions of scatterers, where their positions are essentially uncorrelated and the scattered light waves recover plane wave behavior between successive scattering events ($k_0 l_t \gg 1$). This picture necessarily breaks down at high volume fractions and high scattering strengths of the particles and the density dependence of l_s and l_t must deviate from the ρ^{-1} law characterizing the "dilute" (weak multiple scattering) regime. Imagine, for example, cube-like scatterers progressively filling up space until reaching dense regular packing. In this limit of an optically homogeneous sample, multiple scattering would disappear and l_t tend to ∞. There is a simple way to include the effects of interparticle correlations for large $k_0 l_t$ [24,37,38,25,39]: Since the *single* scattering intensity from correlated spherical particles in the far field is given by the product of the form factor $F(q_s)$ and the structure factor $S(q_s)$, which depends on the inter-particle interaction potential, we can consider the multiple scattering as a series of scattering events from groups of correlated particles with angular dependence $F(q_s)S(q_s)$, as long as the range of positional correlations is small compared to l_s. Recall from section 1.1.3 that for negligible correlations l_t and l_s are related by $l_t = l_s/(1 - \langle \cos\theta_s \rangle_{F(q_s)})$. Correlations then require angular average over $F(q_s)S(q_s)$ and, thus, $l_t = l_s/(1 - \langle \cos\theta_s \rangle_{F(q_s)S(q_s)})$. Since $(1 - \cos\theta_s) \propto q_s^2$ the relative correction of l_t due to correlations is

$$\frac{l_t}{l_t'} = \frac{\int_0^{2nk_0} q_s^2 F(q_s) S(q_s) q_s \, dq_s}{\int_0^{2nk_0} q_s^2 F(q_s) q_s \, dq_s} \tag{2.5}$$

This correction, using the Percus–Yevick structure factor $S(q_s)$ for hard spheres, quantitatively describes the volume fraction (vf.) dependence of l_t in aqueous suspensions of colloidal latex spheres up to almost 50% [25,39]. The deviation from the ρ^{-1}-dependence becomes significant above about 15% vf. and $l_t/l_t' \approx 0.5$ at 45% vf. in this system. It may become much larger for high index particles such as TiO_2 as illustrated in fig. 3.

Kaplan et al. [40] have extended the description of interparticle correlations to binary mixtures of hard spheres of two different sizes where three partial structure

* For example closed paths with identical first and last scatterer.

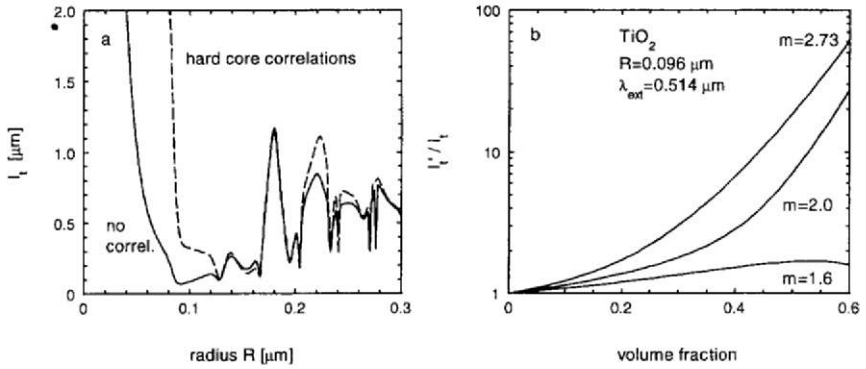

Fig. 3. Estimation, using eq. 2.5, of the effect of interparticle correlations on l_t for colloidal TiO_2 particles at $\lambda = 0.514$ μm. l_t (—— no correlations) and l_t' (- - - - correlations). (a) Size dependence of l_t and l_t'. (b) l_t'/l_t vs. volume fraction at different index mismatch m.

factors come in. Here again, good agreement with l_t'-measurements on aqueous suspensions of latex particles was found over the investigated range of particle diameters and mixing fractions.

2.3. Polarization

The scattering matrix in section 1.1 shows that the polarization state of the light is generally changed on scattering, both for Rayleigh and Mie-particles. For spheres, the change depends only on the incident polarization state and on the direction of the outgoing wave vector. In our description of light propagating along random multiple scattering paths, we are interested in the evolution of the polarization state along a path, the state being defined with respect to the local direction of propagation. This evolution is completely determined by the configuration of the path and is obtained, in principle, by multiplication of the successive scattering matrices expressed in the local coordinate frame. However, because of the complexity of this in the case of high order Mie scattering, a discussion appears impossible within the constraints of this course (see e.g. [41,20,12,42]). Rather, a few statements are made and illustrated by examples.

Inspection of a cloud through a polarizer sheet shows that high order multiple scattering completely "depolarizes", the memory of the incident polarization state is lossed. The sun light multiply scattered through a cloud contains in fact a mixture of *all* polarization states. This is in contrast to coherent light* where each speckle spot has a well defined, but different polarization state because of

* With coherence length longer than the characteristic path length.

the *coherent* superposition of the fields scattered along different paths in a given direction [12]. In both cases, the randomization of the incident polarization state occurs on a characteristic length scale which is typically, but not necessarily, of the order of l_t (decay length of $\boldsymbol{k_o}$). Imagine for instance a two-dimensional disordered array of scatterers. In this case light with linear polarization normal to the layer and diffusive propagation in the plane will *not* depolarize even over macroscopic distances. Single backscattering preserves linear polarization, but flips the helicity of circular polarization. Thus, the characteristic decay length for polarization depends on the incident polarization state itself and, in addition, on parameters of the scatterers such as their size which determines the relative amount of forward to backward scattering. Once the light has penetrated the (3D) multiple scattering medium by many polarization decay lengths the random polarization states are widely distributed and a mean polarization decay length may be defined by averaging over the distribution of the polarization states, which is given by a homogeneous density of polarization states on the Poincaré sphere [42].

The coherent backscattering cone has been studied for various polarization states of incident and detected light, respectively [18,41,21,30,20,24] It has been shown [20] that for spherical Rayleigh, Rayleigh–Gans and Mie scatterers full coherence between the reversed paths prevails for parallel linear polarized incident and detected light. Therefore an enhancement factor of two and a cone shape very similar to the scalar wave prediction is expected, in agreement with experiment. The small and broad cones observed for perpendicular linear polarizations of incident and detected beam, respectively, are non-universal and related to the partial coherence of particular low order scattering paths. The use of identical circular polarizers for incident and detected beam provides not only an enhancement factor of two, in principle, but is also a convenient experimental tool to suppress single backscattering, which flips the helicity [29]. This is most useful for Rayleigh particles which have higher direct backscattering cross sections than Mie particles.

2.4. *Magneto-optical Faraday effect*

As already recognized by Faraday and shown experimentally by Rayleigh [43] the magneto-optical Faraday effect, i.e. the magnetic field ($\boldsymbol{B}$) induced rotation $\alpha = V\boldsymbol{B}\boldsymbol{s}$ of linear polarized light propagating along $\boldsymbol{s}$, changes sign on reversal of $\boldsymbol{s}$. Hence, the Faraday effect acts like an optical diode* and should therefore destroy coherent backscattering [44,45]. The first theories [44,45] of this effect assume, that the Faraday rotation increases proportional to the dis-

* This property is often used in optical "insulators".

tance between scattering events but is randomized at each scattering by a random helicity flip. In fact, the (Faraday) rotation is not *randomized* at all on each scattering event, but transformed in a deterministic, $\boldsymbol{k}$-dependent way because of the completely deterministic transformation of the polarization on scattering (see section 2.3) [46]. For random paths in 3D, one might expect that it accumulates along the scattering path over a distance (l_f) comparable with, but not necessarily equal to the average polarization decay length [27] which in turn may differ from l_t. In this simple picture, which is a random walk of the Faraday rotation α with step length l_f on a random walk with step length l_t, the difference in Faraday rotation angle between reversed paths, per step l_f, is of order $\delta\alpha = 2VBl_f \cos\Theta$, Θ being the angle between $\boldsymbol{B}$ and the local direction of propagation. The coherence factor between the time reversed paths for a given step is $\cos\delta\alpha$. For equidistant random steps, this gives a Θ-averaged contribution of $\langle\cos\delta\alpha\rangle_\Theta = u \approx e^{-2V^2B^2l_f^2/3}$ to $i(q)$ per step. For an exponential step length distribution, one obtains $u_g \approx \arctan(2VBl_f)/2VBl_f$ [27]. Under the assumption of no correlations between the $\delta\alpha's$ of consecutive steps, one obtains for paths of length s the average contribution $e^{-s/l_f \cdot \ln u}$. Since the phase shifts between reversed paths due to Faraday rotation are independent of phase shifts due to variations of the external scattering angle θ, we can write for $i(q, B)$ in the presence of a magnetic field

$$i(q,B) = \frac{1}{i(0,0)} \int_{l_t}^{\infty} P(s) \exp[-\frac{s}{3l_t}(q^2 l_t^2 + 3l_t/l_f \ln u)]\, ds. \tag{2.6}$$

Both terms in the exponent have the same s-dependence and therefore, the q-dependence of the cone without Faraday rotation $i(ql_t, 0)$ and the B-dependence of the tip $i(0, \sqrt{3l_t/l_f \ln u})$ should be identical. The data in fig. 4b illustrate that this prediction is in very good agreement with recent experiments [27]. The field induced rounding of the cone at small angles is very analogous to the rounding due to absorption discussed in section 2.1.2. However, as the incoherent wide angle scattered intensity is not affected by Faraday rotation, the enhancement factor is reduced now: The B field operates on the phase, not on the amplitude.

2.5. Long range speckle correlations

We have argued in section 1.3 that the fields scattered along different paths are uncorrelated. Then, all interferences between different paths average out both in the average scattered intensity and in the intensity–intensity correlation function (C). The latter is thus given by $C(x) = \langle E(0) \cdot E^*(x)\rangle_x^2 / \langle E(0)^2\rangle - 1$ where x stands for some quantity introducing phase shifts between the scattering paths, such as *time* for scatterers under motion, *frequency shift* of the incident laser light, *angle*

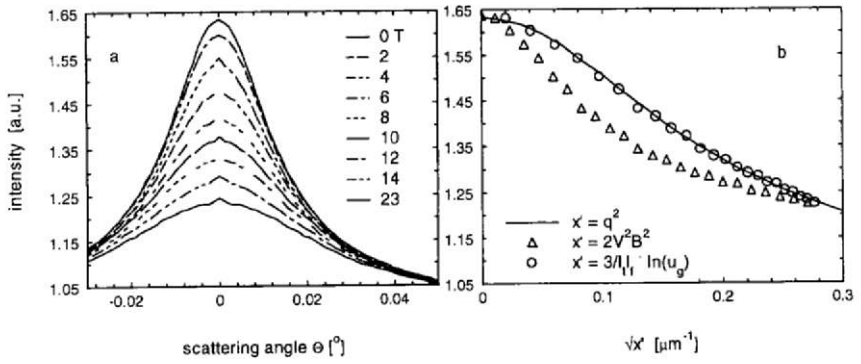

Fig. 4. (a) Destruction of backscattering cones by magnetic fields. Sample: 0.03 μm diameter Si particles at 5% vf. in a rare earth doped glass matrix. $l_t = 110$ μm (b) Comparison of the angular dependence of the zero field cone (cont. line) and the field dependence of the zero angle enhancement factor (dots), when plotted in reduced units as suggested by eq. 2.6.

of incidence and detection, or *magnetic field* in magneto-optically active media. $E(x)$ denotes the total scattered field which is the coherent sum over the fields $E_i(x)$ scattered along the different paths. In this so-called "factorization" approximation, $C(t)$ only contains terms $\langle E_i(0)E_i^*(x)\rangle\langle E_j(0)E_j^*(x)\rangle$, and is again written as a sum over $P(s)$. This contribution to C is denoted C_1.

Correlations between high order multiple scattering paths arise from paths which cross at a certain scattering site [47,48]. This opens the possibility for a non-vanishing contribution of $\langle E_i(0)E_i^*(0)\rangle\langle E_j(x)E_j^*(x)\rangle$ to $C(x)$. In other words, on increasing x the fields E_i and E_i^* do not loose coherence at all between source and crossing point or between crossing point and detector. This contribution $C_2(x)$ to $C(x)$ decays thus more slowly than $C_1(x)$ with increasing x, since the crossing point may be located at any place inside the sample. In addition, $C_2(x)$ does not depend on the angle of incidence, nor on the angle of observation, respectively.

In the less probable case of two crossings of two multiple scattering paths, even more correlations build up giving rise to an additional term $C_3(x)$ in $C(x)$. $C_3(x)$ originates from terms $\langle E_i(0)E_i^*(0)\rangle\langle E_j(x)E_j^*(x)\rangle$ between source and first crossing *and* after second crossing and detector. It decays even more slowly with x than $C_2(x)$ since the path segments between the crossings – where C_3-decorrelation occurs – are shorter on average than those between one crossing and the interface (C_2). Most interestingly, C_3-correlations depend neither on the direction of incidence nor of detection. Therefore they give rise to fluctuations of the angular integrated transmission for diffuse illumination. C_3-fluctuations are independent of the sample size and may be considered

as the optical analogue of the universal conductance fluctuations in electronic systems.

Optical speckle fluctuations are dominated by C_1-fluctuations because of the very small crossing probability of paths in typical experiments on macroscopic samples. As a consequence most experiments on speckle correlation functions are well described by the "factorization" approximation. Examples are the angle–angle correlations (or memory effect) [49,50], the frequency–frequency correlations [51–53], the magnetic field-magnetic field correlations [54] and time–time correlations (see section 3.2). The only observation of optical C_2-fluctuations so far is due to de Boer et al. [52,53], who have found, in addition to a large C_1-signal, the expected small amplitude power law decay in frequency shift using a tunable laser, strongly focussed on very small TiO_2/air samples and collecting the diffuse transmitted light by an integrating sphere which averages over the transmission speckle spots. The corresponding probability distribution of the total transmitted intensity is essentially a Gaussian about the average transmission, as expected, but a small deviation indicating contributions from higher order corrrelations (3 crossing beams) was found [55]. It has not been possible so far to detect the even smaller C_3 term.

2.6. Nonlinear media

Very recently interest has developed in nonlinear properties of disordered media. The shape of the coherent backscattering cone [56–58] and C_1-correlations [59] have been studied for the light generated at the second harmonic frequency inside media consisting of particles with nonlinear susceptibility. The generation of frequency doubled light requires two photons to meet at a given scattering site, and it appears natural to treat this case with the photon diffusion picture but now putting the sources of diffusing 2ω photons distributed within the sample. The $2\omega - C_1$-correlations are therefore long range like C_2-correlations in linear media [59].

In addition, laser action has been studied in mixtures of colloidal suspensions with laser dyes [60–62] and in powders of neodynium crystals [63]. The observed features are essentially consistent with superradiant laser emission*, or amplified spontaneous emission (ASE), caused by scattering paths longer than the characteristic length l_g for positive gain. Strongly scattering media provide those long paths even in samples with relatively small external dimensions. The ASE emission from such samples is non-directional and speckle-like. Like normal speckles, it appears globally incoherent despite of its coherence within each speckle spot. Coherent backscattering also exists for the ASE light [64,65] with an enhance-

* Without external cavity, because there is no!

ment factor close to 2. As l_g can be viewed as a negative absorption length, the cone becomes narrower as opposed to the absorption induced broadening. In analogy to absorption, the narrowing occurs for scattering angles smaller than $\sqrt{l_t/l_g}$ [65].

2.7. *Attempts and difficulties to observe 3D localization of light*

What happens, if the parameter λ/l_t becomes larger? An increasing width of the backscattering cone implies a reduction of the transmitted intensity T according to $T = \frac{l_t}{L}(1-(k_o l_t)^{-2})$ [66]. In this weak localization regime ($\lambda/l_t \ll 1$) the same correction applies to the photon diffusion constant D, since $T = 3D/cL$. On increase of λ/l_t towards 1, the picture of photons diffusing along uncorrelated paths becomes more and more unreliable. The diffusing intensity is reduced by coherent backscattering, particularly for long paths, and the probability of crossings of paths (section 2.5) increases. According to the scaling theory of localization [66] the diffusion constant D becomes scale dependent and near $\lambda/l_t = 1$ (Joffe–Regel criterion [67]) the optical transmission of a macroscopic sample should vanish. John [68] has first pointed out that this peculiar state of light, diffusing without being capable to escape across the sample boundaries, may exist for dense ensembles of dielectric particles. However, the efficiency of light scattering being weak both at small and long wavelengths (see section 1.1), $k_0 l_t$-values of order unity can only be reached in Mie-resonance of high index dielectric particles at very elevated volume fractions. Since, in addition, absorption has to be kept small (which presumably excludes the use of metallic or semiconducting particles) the range of parameters is very restricted and the undesirable effect of interparticle correlations (cf. fig. 3) certainly large.

After the discovery of weak light localization, efforts were made to observe the transition to strong light localization or, at least, to detect the anomalies in light transport in the pretransitional regime. Watson et al. [69] measured D from the broadening of a *psec* pulse transmitted through aqueous latex suspensions, but λ/l_t was much too small. Using a similar technique, Drake and Genack [70] reported very small D-values in dense samples of resonant TiO_2 particles, suggesting the discovery of the anomalous regime near the localization transition. However, combined measurements of D and l_t by van Albada et al. [71] revealed evidence for an almost tenfold lowering of the velocity of transport of the light energy on resonant scattering, while l_t stayed reasonably large. The small energy transport velocity is due to the finite dwell time in resonant scattering: scatterers act as resonators of quality Q which need about Q cycles to be pumped by the light pulse. A theoretical analysis [72] accounts for these observations. Thus, there is no evidence for the onset of light localization in disordered media so far. The difficulty in the highly dense systems is to evaluate experimentally the "clas-

sical" value of l_t and its modification due to interferences. The high field Faraday effect may turn out very useful here, since it selectively destroys the constructive interference between reversed paths.

3. Applications

3.1. Dynamic correlation function of the multiple scattering intensity

We now briefly discuss the effects of motion of the scatterers on the multiple scattering speckle patterns [37,73,74,38,76,77]. It follows from the origin of speckles (section 1.3) that the intensity of individual speckle spots fluctuates when particles change their relative positions, since the phase shifts of the light scattered along the different paths fluctuate. Within the factorization approximation the dynamic correlation function of the intensity scattered in a given speckle spot, $\langle I(0)I(t)\rangle$, can be simply obtained as an *incoherent* sum over the paths length distribution $P(s)$.

$$\langle I(0)I(t)\rangle/\langle I(0)^2\rangle - 1 = |\langle E(0)E^*(t)\rangle|^2/\langle I(0)\rangle^2,$$

where

$$\langle E(0)E^*(t)\rangle = 1/\langle I(0)\rangle \int_{l_t}^{\infty} P(s)\langle E_i(0)E_i^*(t)\rangle.$$

$E_i(t)$ is the electric field scattered along a path (with index i) and $\langle\cdots\rangle$ denotes the average over configurations of paths and over time t. All interferences between different paths average to zero in the correlation function and hence we only need to consider the time dependent phase shifts $\Delta\Phi$ (t) between $E_i(0)$ and $E_i^*(t)$. $\langle E_i(0)E_i^*(t)\rangle = \langle e^{i\Delta\Phi(t)}\rangle = \langle e^{-\Delta\Phi^2(t)}\rangle$. The latter equality follows from the Gaussian distribution of $\Delta\Phi$ due to the random configurations of the paths. At small correlation times t we can write $\langle e^{-\Delta\Phi^2(t)}\rangle \approx e^{-\langle\Delta\Phi^2(t)\rangle}$. For uncorrelated motion of the successive scatterers along a path the total variance of the phase $\langle\Delta\Phi^2(t)\rangle$ is related to the mean square phase per scattering event $\langle\delta\phi^2\rangle$ by $\langle\Delta\Phi^2(t)\rangle = n\langle\delta\phi^2\rangle$. $n = s/l_s$ denotes the number of scattering events along paths of length s. We have thus reduced the expression for the dynamic field correlation function $C(t)$ to the form

$$C(t) = \int_{l_t}^{\infty} P(s)e^{-\frac{s}{l_s}\langle\delta\phi^2\rangle}\,ds/\int_{l_t}^{\infty} P(s)\,ds, \tag{3.1}$$

which is identical to eq. 2.1 describing the angular dependence of the coherent backscattering cone as a sum over $P(s)$. Note that this holds whatever $P(s)$ and $\langle\delta\phi^2\rangle$ are.

3.2. Brownian motion of colloidal scatterers

$\langle \delta\phi^2 \rangle$ is easily obtained for independent particles undergoing Brownian motion. Each scattering event defines a scattering vector $\boldsymbol{q_s}$ and the phase shift associated with a displacement $\delta \boldsymbol{r}(t)$ of a scatterer is $\delta\phi = \boldsymbol{q_s}\delta \boldsymbol{r}(t)$. In single scattering $\langle \delta\phi^2 \rangle = q_s^2 \langle \delta r(t)^2 \rangle = q_s^2 D_0 t$, D_0 being the Stokes diffusion constant of the particles [78]. Unlike in single scattering, q_s in multiple scattering has random directions and a wide distribution of moduli ranging between 0 and $2k_0$. Therefore, $\langle \delta\phi^2 \rangle = \langle q_s^2 \delta r(t)^2 \rangle = \langle q_s^2 \rangle \langle \delta r(t)^2 \rangle$. The latter identity is justified by the fact that the $\boldsymbol{q_s}'s$ and $\delta \boldsymbol{r(t)}'s$ are uncorrelated at short times t. With $\langle q_s^2 \rangle = 2k_0^2 \langle 1 - \cos\theta_s \rangle = 2k_0^2 l_s/l_t$ one obtains $\langle \delta\phi^2 \rangle = (l_s/l_t)(t/2\tau_o)$ where $\tau_0 = 1/(D_0(2k_0)^2)$ is the characteristic correlation time for *single* backscattering. Insertion of $\langle \delta\phi^2 \rangle$ in eq. 3.1 shows several interesting features. *First*, l_s drops out and $C(t)$ is controlled by the decorrelation on the scale of the *transport* mean free path l_t. This is very convenient in the evaluation of $C(t)$ since in the diffusion picture $P(s)$ is also a function of l_t, but not of l_s. *Second*, the light scattered on long paths decorrelates faster than the contributions from short paths. Physically, for a speckle spot to significantly change its intensity, the phases of the contributing fields need to change by about 2π, which is achieved earlier for longer paths, since phase shifts accumulate proportional to the number of scattering events along the paths. The important implication of this is that in dynamic multiple scattering particle motion is probed at distance scales *shorter* than the optical wavelength. Depending on the typical path length probed experimentally (which can be adjusted by sample size, reflection or transmission geometry, absorption etc.) motion can be measured from a μm scale down to a nm scale or even below. For example, in transmission through a slab, the dominant path length is of order L^2/l_t and thus $C(t)$ decays on a time scale $\tau_0(l_t/L)^2$, which may be typically $< 10^{-5}\tau_0$. *Third*, $3t/2\tau_0$ in eq. 3.1 is equivalent to ql_t in eq. 2.1 (or to $3l_t/l_a$ in the case of absorption) and, therefore, the t-dependence of $C(t)$ is identical to the q^2-dependence of $i(q)$ and to the $1/l_a$-dependence of $i(0)$. The expressions for $i(q)$ discussed above immediately provide a simple theory for $C(t)$, which has, obviously, the same advantages and shortcomings than those discussed in section 2.1.1. Recent random walk simulation work [79] suggests that the diffusion theory provides accuracy to within a few % for typical experimental parameters.

The first experiments of dynamic multiple light scattering [37,74] which where carried out on colloidal latex suspensions at vf. above a few % in backscattering and transmission confirmed the above features, including the effects of finite sample size [74], finite laser coherence length [75], finite absorption length [76] and the analogy between $C(t)$ and $i(q)$ [76]. As all required parameters $(\gamma, l_t, L, \tau_0, l_a, \ldots)$ could be obtained either experimentally or from Mie scattering, the comparison between theory and experiment was found to hold quantit-

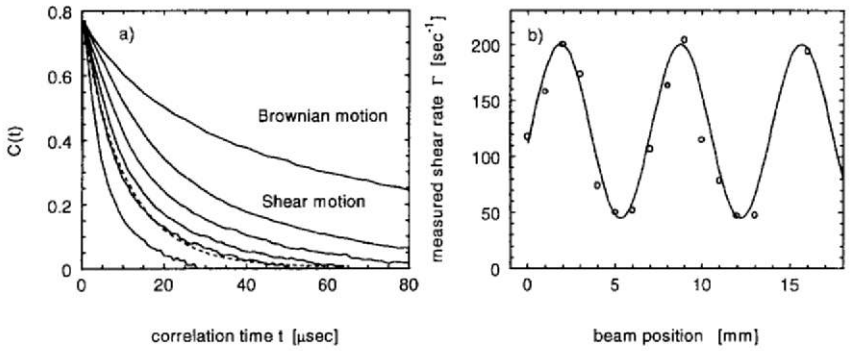

Fig. 5. (a) $C(t)$ of a suspension of $0.28\mu m$-diameter TiO_2-particles at 0.117% vf. in reflection. Top to bottom: Planar shear at rate ($\Gamma = 0, 27, 43, 62, 80, 137$ sec^{-1}). (- - - -) theory, see section 3.3 (b) Γ depends on the position of the laser beam revealing Taylor rolls, $L = 34$ mm [92].

atively to within 10%. This novel dynamic multiple light scattering technique is often called "diffusing-wave spectroscopy, DWS".

3.2.1. Particle sizing

It is thus possible to determine the hydrodynamic radius R of the scatterers from a measurement of τ_0 in "white" suspensions which are not too concentrated (typically $\approx 1\%$ vf.), so that the diffusion constant is given by Stokes' formula $D_0 = kT/6\pi\eta R$. Experiments on monodisperse particles with different size have shown [37,24,74,76,77] that the t/τ_0-scaling works both in backscattering and in transmission and the decay of $C(t)$ is well described by the diffusion model. An example is shown in fig. 5a. However, attention must be paid to account for single and low order multiple scattering which are not included in the model but may add significantly to the data [75,80]. Single scattering is easily suppressed in backscattering by using circularly polarized light of identical helicity in incident and detected beam. In cases of negligible low order contributions experimental γ-values range from 0.6 to 0.8. An elegant way to eliminate the uncertainty due to γ (section 2.1.1) is to use monomode optical fibers for injection and detection of the light deep inside the sample [81]. In this case, the $P(s)$ to be used in $C(t)$, eq. 3.1, is given by eq. 1.5. Large multimode fiber bundles used for injection and detection approaches the case of planar incident and detected wave (eq. 1.7) [82]. It is interesting to note that a comparison of *dynamic* $C(t)$ data obtained in transmission and reflection on the same sample provides a measurement of the *static* quantity l_t. One of the drawbacks of dynamic multiple light scattering is its lack of sensitivity to polydispersity of the particle size: On their multiple scattering paths photons scan the size distribution of scatterers and the measured relaxation rate is a (l_t^{-1})-weighted average of the $1/\tau_0$'s.

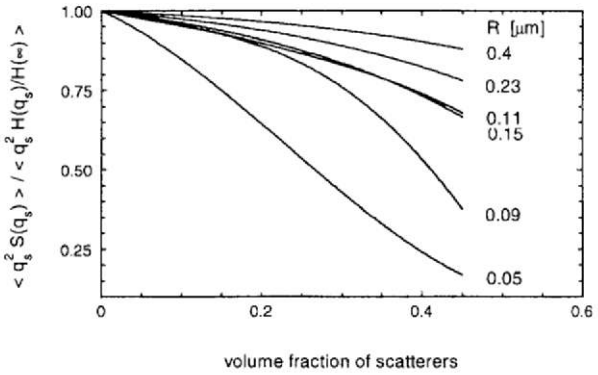

Fig. 6. Effect of hydrodynamic and static hard core interparticle correlations on the average dynamic relaxation rate normalized to D_s/D_0 (eq. 3.2) per scattering event in high order multiple scattering for various size polystyrene spheres in water at $\lambda = 0.514$ μm.

3.2.2. Interparticle correlations

For weak scattering, $k_0 l_t' \gg 1$, the effects of interparticle interactions (section 2.2) are easily extended to dynamic multiple scattering [37,38,75]. It is well known that the relaxation rate of $C(t)$ in *single* scattering from monodisperse interacting spherical particles is given by $D(q_s)q_s^2 = D_0 q_s^2 H(q_s)/S(q_s)$ where hydrodynamic correlations are described by $H(q_s)$, and the short time diffusion coefficient is $D_s = D_0 H(\infty)$. In multiple scattering, the groups of correlated particles acting as effective scatterers modify the average relaxation rate $D_0\langle q_s^2\rangle_{F(q_s)}$, which becomes $\langle D(q_s)q_s^2\rangle_{F(q_s)S(q_s)}$. Inserting this expression and the correction of l_t (eq. 2.5) into eq. 3.1 provides a correlation induced relative change of $1/\tau_0$

$$\frac{\tau_0}{\tau_0'} = \frac{D_s}{D_0}\frac{\displaystyle\int_0^{2nk_0} q_s^2 \frac{H(q_s)}{H(\infty)} F(q_s) q_s dq_s}{\displaystyle\int_0^{2nk_0} q_s^2 S(q_s) F(q_s) q_s dq_s} \tag{3.2}$$

The first factor (D_s/D_0) reflects the effect of hydrodynamic interaction on the short time diffusion constant, irrespective of whether or not the sample multiply scatters light, and the second describes the multiple scattering correction through a modification of $\langle q_s^2\rangle$. The latter term evaluated for hard monodisperse spheres [25,83] is shown in fig. 6 for various sphere sizes as a function of the particle volume fraction. The influence of interactions becomes pronounced at high volume fractions and small particle size, but almost disappears for particles above $\approx 1\mu m$ diameter: For large particles the oscillations in $S(q_s)$ and $H(q_s)$

are at small q_s so that they more efficiently average in the integrals of eq. 3.2 than for small particles. Knowing this correction a measurement of $C(t)$ allows to determine D_s up to very high ($\approx 50\%$) volume fractions. This has been demonstrated first by Fraden [25] and Qiu [83]. The smallness of the multiple scattering correction for large spheres was exploited to study $H(q_s)$ to some extent [84]. Measurements of $C(t)$ have been extended to binary mixtures [40] of colloidal spheres, but in this case a quantitative comparison with theory suffers from the lack of expressions for $H(q)$. At even higher concentrations binary mixtures or monodisperse suspensions undergo, respectively, a glass [85] or crystal [86] transition visible by the appearance of a long time tail in $C(t)$ which is very useful to establish phase diagrams.

3.2.3. Short time dynamics

The fact that DWS probes motion at much smaller distance and time scales than conventional dynamic light scattering has been exploited to study the cross over from ballistic to diffusive motion of spheres [87] and has provided evidence for long time power law behavior of the velocity correlation function which scales with the fluid viscosity [88]. DWS has also been used to study the effect of hydrodynamic interactions on the sedimentation velocity, its variance and diffusion in fluidized suspensions [89].

3.3. Convective motion

Multiple scattering speckles are sensitive to relative motion of scatterers other than Brownian motion. This was first illustrated by $C(t)$ measurements on latex suspensions under Poiseuille flow [90]. If the particle's displacements $\delta \boldsymbol{r_i}$ are not independent but completely correlated due to (deterministic) convective flow, the relevant phase shift $\delta\phi$ due to two successive scattering events (i) and $(i+1)$ in the expression for $C(t)$ is $\boldsymbol{k_i}(\delta \boldsymbol{r_i} - \delta \boldsymbol{r_{i+1}})$. Since $\delta \boldsymbol{r_i} = \boldsymbol{v_i} t$, it immediately follows that a homogeneous velocity field $\boldsymbol{v_i} = const.$ does not generate temporal speckle fluctuations. Inhomogeneous velocities, however, cause phase fluctuations. These are given by the velocity difference on the length l_s, since consecutive scattering events have on average a distance l_s. For uncorrelated successive scattering events ($l_s = l_t$) and homogeneous shear at rate Γ one again finds the familiar expression (eq. 3.1) for $C(t)$, the mean square phase shift per step now being $\langle \delta\phi^2 \rangle = (t/\tau_s)^2$. The characteristic rate is $1/\tau_s = \Gamma l_t k_0/\sqrt{30}$ and the numerical factor $\sqrt{30}$ results from angular averaging. The t^2 dependence of $\langle \delta\phi^2 \rangle$ - as opposed to the t-dependence for random motion – is the signature of the deterministic nature of the shear motion. For inhomogeneous shear such as Poiseuille flow or plug flow the decay of $C(t)$ somewhat deviates from the above form, since the cloud of diffusing photons does not scan the different regions

of the flow field with equal weight [91]. Recent experiments comparing planar flow, Poiseuille flow and Couette flow [92] confirm this and are in quantitative agreement with theory. It is thus possible to distinguish different types of flow and to determine shear gradients in turbid liquids by dynamic light scattering. In transmission through a slab this can be done even without detailed knowledge of the multiple scattering properties of the sample as l_t essentially drops out of the expression for $C(t)$. The Couette experiments have been extended to higher Γ values into the regime of hydrodynamic instabilities [92]. Above a critical shear rate, a characteristic convective roll pattern (so-called Taylor rolls) appears. The associated additional shear is clearly seen in $C(t)$, and by focusing the incident beam to an area smaller than the roll diameter and scanning the incident beam position makes possible to visualize the otherwise invisible rolls through the position dependence of τ_s. An example is shown in fig. 5b. These experiments can be extended to turbulent flow opening the possibility of scale dependent measurements of $\langle \Gamma^2 \rangle$ [93].

Longitudinal relative displacements of the particles generated by ultrasonic waves modulate multiple scattering speckle patterns in a very similar way and by comparison of theory and data the ultrasound amplitude can be estimated optically in turbid solid or liquid media [94].

3.4. Recent applications of "diffusing wave spectroscopy"

After the establishment of the principles of dynamic multiple light scattering on well characterized model suspensions more complex turbid systems begin to be studied. Among the large number of interesting materials we emphasize emulsions, paints, foams, dairy products and biological tissue. Coarsening and aging of foams has been investigated by Durian et al. [95,96] describing the dynamics as a stochastic sequence of bubble rearrangement events which – despite of their rare occurrence – are easily detected by the extended photon cloud . Similar measurements were performed recently on flowing foam [97]. Experiments on very dense suspensions of monodisperse emulsion droplets provide evidence for droplet shape fluctuations with amplitudes as small as a few Å at a droplet size above $1\mu m$ [98]. Another example is the monitoring of gelation of milk by rennet action as an early stage in cheese production [99].

3.5. Imaging through turbid media

The recent progress in coherent and incoherent light transport through turbid media has initiated substantial work on imaging "beyond one transport mean free path". The central question is how well can an object be located when buried (in this sense) deep inside the medium. Two approaches can be distinguished,

roughly: analyzing (1) all diffusing photons, or (2) only the ballistic and "snake-like" photons which have not completely lossed directional information. In (1) the object differs from the turbid medium either by enhanced transparency or enhanced absorption and therefore modifies the photon cloud. It acts as a sort of source or sink for diffusing photons and therefore generates a glow or shadow, respectively, on the sample surface. These features are less pronounced and broader for deeply buried objects than for objects near the surface, since photons passing by the object spread in a cone of $\approx 90°$ opening towards the surface. Thus, the width of the feature allows to estimate the depth location of the object while its in plane location is given by the center of gravity of glow or shadow [100]. In other words, the spatial resolution degrades linearly with the distance from the surface. Speckle tomography [101–103] works along the same lines; if the object – which in this case may be undistinguishable from the medium - is moved, the corresponding changes of the speckle pattern are most pronounced in the surface region closest to it. In the second approach (2) the "direct" photons are separated from the diffusing photons either by time gating the early arriving photons in a pulse experiment [104], or by coherent (heterodyne) detection of the high frequency modulated incident beam. In (2) the detected signal decays exponentially with the sample thickness, but because of the high sensitivity of optical detectors ($T \approx 10^{-10}$ detectable) sharp images over 10 to 100 scattering mean free paths may be obtained.

3.6. Medical applications

Biological tissue looks turbid and opaque because of strong scattering and strong absorption in the visible. There is, however, a window of relatively low extinction in the near infrared, with l_t-values of some $100\mu m$ to some mm or more [105]. This allows to apply the imaging concepts discussed in section 3.5 to visualize or locate contrasted objects such as blood vessels, coagulates or dye-stained tumors even a few cm deep inside the body. Although one has little hope so far for the emerging imaging devices to compete with NMR or X-ray imaging techniques in terms of in depth resolution and polyvalent use, their expected low cost and spectroscopic resolution may result in useful specific diagnostic devices.

4. Conclusion: light versus electrons

This lecture has illustrated analogies and differences between multiple scattering of light and electrons. They are summarized here in terms of advantages and disadvantages of light versus electron scattering:

For the case of light. Single scattering is well understood for many types of particles. Well characterized scatterers are available (particle's size, shape, refractive index, absorption coefficient, density can be tailored at will.). The mean free paths l_s and l_t are precisely calculated and easily adjustable for many systems. Inter-particle correlations are controllable and well described theoretically for spheres. The coherence lengths of lasers are much larger than typical multiple scattering paths, there are always interference effects. Making mesoscopic optical samples ($L \approx l_t$) or ($L \approx \lambda$) with well defined geometry is possible. The small divergence and extreme monochromasy of laser beams combined with small detectors provide almost arbitrarily good directional control allowing for the study of single channels (speckle spots). High resolution spectroscopic techniques are available for precise measurements of frequency correlations, time of flight or particle motion. Absorption and incoherent scattering can be made negligible, which is equivalent to "zero" temperature in electronic systems. Last but not least there is no photon photon interaction.

Against the case of light. Scattering is more complex due to the vector wave nature of light. The optical scattering efficiency is weak, in particular at small energies (Rayleigh regime); therefore strong light localization seems very difficult to reach, and – if at all – only in a small window of parameters. The coupling to magnetic fields via the Faraday effect is weak.

References

[1] Physics Today, Dec. 1988, Special Issue: *Disordered Solids.*
[2] P. Sheng, ed., *Scattering and Localization of Classical Waves in Random Media*, (World Scientific, Singapore, 1990).
[3] S. John, Physics Today, May (1991) 32–40.
[4] G. Maret, Phys. Bl. **48** (1992) 161.
[5] C.M. Soukoulis (Ed.): *Photonic band gaps and localization*, Nato ASI Series B, Physics **308** (Plenum, N.Y., 1993).
[6] H.C. van de Hulst, *Light Scattering from Small Particles* (Dover, N.Y., 1981).
[7] M. Kerker, *The Scattering of Light and Other Electromagnetic Radiation* (Academic, N.Y., 1969).
[8] A. Ishimaru, *Wave Propagation and Scattering in Random Media*, Vol. I, II (Academic, N.Y., 1978).
[9] S. Chandrasekhar, *Radiative Transfer* (Dover, N.Y., 1960).
[10] C. Dainty, ed., *Laser Speckle and Related Phenomena,* Topics in Applied Physics, Vol. 9 (Springer, Berlin, 1984).
[11] A. Schuster, Astrophys. J. **21** (1905) 1.
[12] S.M. Cohen, D. Eliyahu, I. Freund and M. Kaveh, Phys. Rev. A. **43** (1991) 5748.
[13] E. Akkermans and R. Maynard, J. Phys. (France) **46** (1985) L-1045.
[14] K.M. Watson, J. Math. Phys. **10** (1969) 688.

[15] D.A. de Wolf, IEEE Trans. Antennas Propag. **19** (1971) 254.
[16] Y. Kuga and A. Ishimaru, J. Opt. Soc. Am. **A1** (1984) 831.
[17] M.P. van Albada and A. Lagendjik, Phys. Rev. Lett. **55** (1985) 2692.
[18] P.E. Wolf and G. Maret, Phys. Rev. Lett. **55** (1985) 2696.
[19] E. Akkermans, P.E. Wolf and R. Maynard, Phys. Rev. Lett. **56** (1986) 1471.
[20] E. Akkermans, P.E. Wolf, R. Maynard and G. Maret, J. Phys. France **49** (1988) 77.
[21] M.B. van der Mark, M.P. van Albada and A. Lagendijk, Phys. Rev. B **37** (1988) 3575.
[22] V.D. Ozrin, Physics Letters A **162** (1992) 341.
[23] J.H. Li, A.A. Lisyanski, T.D. Cheung, D. Livdan and A.Z. Genack, Europhys. Lett. **22** (1993) 675.
[24] P.E. Wolf, G. Maret, E. Akkermans and R. Maynard, J. Phys. France **49** (1988) 63.
[25] S. Fraden and G. Maret, Phys. Rev. Lett. **65** (1990) 512.
[26] R. Lenke and G. Maret, Physica Scripta T **49** (1993) 605.
[27] R. Lenke and G. Maret, in ref. [105], pp. 16.
[28] D.S. Wiersma, M.P. van Albada, B.A. van Tiggelen and A. Lagendijk, Phys. Rev. Lett. **74** (1995) 4193.
[29] S. Etemad, R. Thompson, M.J. Andrejco, S. John and F.C. MacKintosh, Phys. Rev. Lett. **59** (1987) 1420.
[30] M. van Albada, M.B. van der Mark and A. Lagendijk, Phys. Rev. Lett. **58** (1987) 361.
[31] A. Lagendijk, R. Vreeker and P. De Vries, Phys. Lett. A **136** (1989) 81.
[32] I. Freund and R. Berkovits, Phys. Rev. B **41** (1990) 496.
[33] J.X. Zhu, D.J. Pine and D.A. Weitz, Phys. Rev. A **44** (1991) 3948.
[34] Th.M. Nieuwenhuizen and J.M. Luck, Phys. Rev. E **48** (1993) 569.
[35] M. Ospeck and S. Fraden, Phys. Rev. E **49** (1994) 4578.
[36] D. Durian, Phys. Rev. E **50** (1994) 857.
[37] G. Maret and P.E. Wolf Z. Phys. B **65** (1987) 409.
[38] F.C. MacKintosh and S. John, Phys. Rev. B **40** (1989) 2383.
[39] P.M. Saulnier, M.P. Zinkin and G.H. Watson, Phys. Rev. B **42** (1990) 2621.
[40] P.D. Kaplan, A.G. Yodh and D.J. Pine, Phys. Rev. Lett. **68** (1992) 393.
[41] M.J. Stephen and M.J. Cwilich, Phys. Rev. B **34** (1986) 7564.
[42] A. Martinez and R. Maynard, in ref. [5]
[43] Lord Rayleigh, Phil. Trans. **176** (1885) 343, and Scientific Papers **2** (1900) 360, and **3** (1902) 163, Cambridge.
[44] A.A. Golubentsev, Sov. Phys. JETP **59** (1984) 26.
[45] F.C. MacKintosh and S. John, Phys. Rev. B **37** (1988) 1884.
[46] A. Martinez and R. Maynard, Phys. Rev. B **50** (1994) 3714.
[47] M.J. Stephen and G. Cwilich, Phys. Rev. Lett. **59** (1987) 285.
[48] S. Feng, C. Kane, P.A. Lee and A.D. Stone, Phys. Rev. Lett. **61** (1988) 834.
[49] I. Freund, M. Rosenbluh and S. Feng, Phys. Rev. Lett. **61** (1988) 2328.
[50] R. Berkovits, M. Kaveh and S. Feng, Phys. Rev. B **40** (1989) 737.
[51] A.Z. Genack and M. Drake, Europhys. Lett. **11** (1990) 331.
[52] M.P.van Albada, J.F. de Boer and A. Lagendijk, Phys. Rev. Lett. **64** (1990) 2787.
[53] J.F. de Boer, M.P. van Albada and A. Lagendijk, Phys. Rev. B **45** (1992) 658.
[54] H. Erbacher, R. Lenke and G. Maret, Europhys. Lett. **21** (1993) 5.
[55] J.F. de Boer, M.C.W. van Rossum, M.P. van Albada, Th.M. Nieuwenhuizen and A. Lagendijk, Phys. Rev. Lett. **73** (1994) 2567.
[56] V.M. Agranovich and V.E. Kravtsov, Sov. Phys. JETP **68** (1989) 272.
[57] V.E. Kravtsov, V.M. Agranovich and K.I. Grigorishin, Phys. Rev. B **44** (1991) 4931.
[58] A. Heiderich, R. Maynard and B.A. van Tiggelen, Opt. Comm. **115** (1995) 392.

[59] J.F. de Boer, A. Lagendijk and R. Sprik, Phys. Rev. Lett. **71** (1993) 3947.
[60] N.M. Lawandy, R.M. Balachandran, A.S.L. Gomes and E. Sauvain, Nature **368** (1994) 436.
[61] A.Z. Genack and M. Drake, Nature **368** (1994) 400.
[62] D.S. Wiersma, M.P. van Albada and A. Lagendijk, Nature (1995) in press.
[63] C. Gouedard, D. Husson, C. Sauteret, F. Auzel and A. Migus, J. Opt. Soc. Am. B. **10** (1993) 2358.
[64] A.Y. Zyuzin, Europhys. Lett. **26** (1994) 517.
[65] D.S. Wiersma, M.P. van Albada and A. Lagendijk, Phys. Rev. Lett. **75** (1995) 1739.
[66] P.W. Anderson, Phil. Mag. **52** (1985) 505.
[67] A.F. Joffe and A.R. Regel, Progr. Semicond. **4** (1960) 237.
[68] S. John, Phys. Rev. Lett. **53** (1984) 2169.
[69] G.H. Watson, P.A. Fleury and S.L. McCall, Phys. Rev. Lett. **58** (1987) 945.
[70] J.M. Drake and A.Z. Genack, Phys. Rev. Lett. **63** (1989) 259.
[71] M.P. van Albada, B.A. van Tiggelen, A. Lagendijk, and A. Tip, Phys. Rev. Lett. **66** (1991) 3131.
[72] B.A. van Tiggelen, A. Lagendijk, M.P. van Albada and A. Tip, Phys. Rev. B **45** (1992) 233.
[73] M.J. Stephen, Phys. Rev. B. **37** (1988) 1.
[74] D.J. Pine, D.A. Weitz, P.M. Chaikin and E. Herbolzheimer, Phys. Rev. Lett. **60** (1988) 1134.
[75] P.E. Wolf and G. Maret, in: *Recent Progress in Surface and Volume Scattering*, M. Nieto-Vesperinas and J.C. Dainty, eds. (Elsevier Science Publ., North Holland, 1990) p. 37
[76] D.J. Pine, D.A. Weitz, G. Maret, P.E. Wolf, E. Herbolzheimer and P. Chaikin, in ref. [2]
[77] D.A. Weitz and D.J. Pine, in: *Dynamic light scattering*, W. Brown, ed. (Oxford U. Press, New York 1993) Chapter 16.
[78] B.J. Berne and R. Pecora, *Dynamic Light Scattering* (Wiley, New York, 1976).
[79] D.J. Durian, Preprint.
[80] F.C. MacKintosh, J.X. Zhu, D.J. Pine and D.A. Weitz, Phys. Rev. B **40** (1989) 9342.
[81] E.R. Van Keuren, H. Wiese and D. Horn, Coll. Surf. A: Physicochem. & Engin. Aspects **77** (1993) 29.
[82] D.S. Horne, J. Phys. D: Appl. Phys. **22** (1989) 1257.
[83] X. Qiu, X.L. Wu, J.Z. Xue, D.J. Pine, D.A. Weitz and P.M. Chaikin, Phys. Rev. Lett. **65** (1990) 516.
[84] J.Z. Xue, X.L. Wu, D.J. Pine, and P.M. Chaikin, Phys. Rev. A **45** (1992) 989.
[85] A. Meller and J. Stavans, Phys. Rev. Lett. **68** (1992) 3646.
[86] S. Sanyal, A.K. Sood, S. Ramkumar, S. Ramaswamy and N. Kumar, Phys. Rev. Lett. **72** (1994) 2963.
[87] D.A. Weitz, D.J. Pine, P.N. Pusey and R.J.A. Tough, Phys. Rev. Lett. **63** (1989) 1747.
[88] J.X. Zhu, D.J. Durian, J. Müller, D.J. Weitz and D.J. Pine, Phys. Rev. Lett. **68** (1992) 2559.
[89] J.Z. Xue, E. Herbolzheimer, M.A. Rutgers, W.B. Russel and P.M. Chaikin, Phys. Rev. Lett. **69** (1992) 1715.
[90] X.L. Wu, D.J. Pine, P.M. Chaikin, J.S. Huang and D.A. Weitz, J. Opt. Soc. Am. **B7** (1990) 15.
[91] D. Bicout, E. Akkermans and R. Maynard, J. Phys. France I **1** (1991) 471.
[92] D. Bicout and G. Maret, Physica A **210** (1994) 87.
[93] D. Bicout and R. Maynard, Physica B **204** (1995) 20.
[94] W. Leutz and G. Maret, Physica B **204** (1995) 14.
[95] D.J. Durian, D.A. Weitz and D.J. Pine, Science **252** (1991) 686.
[96] D.J. Durian, D.A. Weitz and D.J. Pine, Phys. Rev. A **44** (1991) R7902.
[97] J.C. Earnshaw and A.H. Jaafar, Phys. Rev. E **49** (1994) 5408.
[98] H. Gang, A.H. Krall and D.A. Weitz, Phys. Rev. Lett. **73** (1994) 3435.
[99] D.S. Horne and C.H. Davidson, Milchwissenschaft **45** (1990) 712.

[100] P.N. DenOuter, Th.M. Nieuwenhuizen and A. Lagendijk, J. Opt. Soc. Am. A **10** (1993) 1209.
[101] R. Berkovits and S. Feng, Phys. Rev. Lett. **65** (1990) 3120.
[102] R. Freund, Phys. Lett. A **147** (1990) 502.
[103] C. Vanneste, S. Feng and D. Sornette, Europhys. Lett. **24** (1993) 339.
[104] D.A. Benaron and D. Stevenson, Science **259** (1993) 1463.
[105] See e.g. OSA Proc. on *Advances in Optical Imaging and Photon Migration*, R.R. Alfano, ed. (Optical Society of America, Washington, DC, 1994), Vol. 21.